

# A Silicate/Glycine Switch To Control the Reactivity of Layered Iron(II)–Iron(III) Hydroxides for Dechlorination of Carbon Tetrachloride

Weizhao Yin,<sup>†,‡,§</sup> Jing Ai,<sup>‡</sup> Li-Zhi Huang,<sup>\*,§,||</sup> Dominique J. Tobler,<sup>⊥</sup> and Hans Christian B. Hansen<sup>‡,§</sup>

<sup>†</sup>School of Environment, Jinan University, Guangzhou 510632, China

<sup>‡</sup>Department of Plant and Environmental Sciences, Faculty of Life Sciences, University of Copenhagen, Thorvaldsensvej 40, DK-1871 Frederiksberg C, Denmark

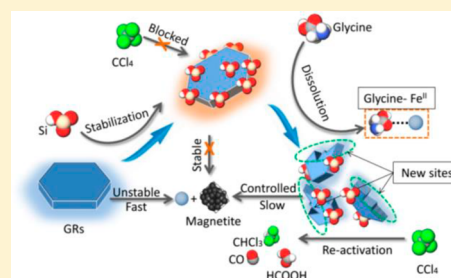
<sup>§</sup>School of Civil Engineering, Wuhan University, No. 8, East Lake South Road, Wuhan, China

<sup>||</sup>Interdisciplinary Nanoscience Center, Aarhus University, Gustav Wieds Vej 14, DK-8000 Aarhus C, Denmark

<sup>⊥</sup>Nano-Science Center, Department of Chemistry, University of Copenhagen, Universitetsparken 5, DK-2100, København Ø, Denmark

## Supporting Information

**ABSTRACT:** Layered Fe<sup>II</sup>–Fe<sup>III</sup> hydroxide chloride (chloride green rust, GR<sub>Cl</sub>) has high reactivity toward reducible pollutants such as chlorinated solvents. However, this reactive solid is prone to dissolution, and hence loss of reactivity, during storage and handling. In this study, adsorption of silicate (Si) to GR<sub>Cl</sub> was tested for its ability to minimize GR<sub>Cl</sub> dissolution and to inhibit reduction of carbon tetrachloride (CT). Silicate adsorbed with high affinity to GR<sub>Cl</sub> yielding a sorption maximum of 0.026 g of Si/g of GR<sub>Cl</sub>. In the absence of Si, the pseudo-first-order rate constant for CT dehalogenation by GR<sub>Cl</sub> was 2.1 h<sup>-1</sup>, demonstrating very high reactivity of GR<sub>Cl</sub> but with substantial Fe<sup>II</sup> dissolution up to 2.5 mM. When Si was adsorbed to GR<sub>Cl</sub>, CT dehalogenation was blocked and Fe<sup>II</sup> dissolution extent was reduced by a factor of 28. The addition of glycine (Gly) was tested for reactivation of the Si-blocked GR<sub>Cl</sub> for CT dehalogenation. At 30 mM Gly, partial reactivation of the GR<sub>Cl</sub> was observed with pseudo-first-order rate constant for CT reduction of 0.075 h<sup>-1</sup>. This blockage and reactivation of GR<sub>Cl</sub> reactivity demonstrates that it is possible to design a switch for GR<sub>Cl</sub> to control its stability and reactivity under anoxic conditions.



## INTRODUCTION

Layered Fe<sup>II</sup>–Fe<sup>III</sup> hydroxides (green rusts) are among the most highly reactive Fe<sup>II</sup>-bearing minerals for reduction of contaminants such as nitrate, nitro aromatic compounds, and chlorinated solvents.<sup>1–4</sup> Green rusts (GRs) have the general composition [Fe<sup>II</sup><sub>(1-x)</sub>Fe<sup>III</sup><sub>x</sub>(OH)<sub>2</sub>]<sup>x+</sup> [A<sup>y-</sup><sub>x/y</sub>·mH<sub>2</sub>O]<sup>x-</sup>, where *x* is the ratio Fe<sup>III</sup>/(Fe<sup>III</sup> + Fe<sup>II</sup>), A is a *y*-valent anion (e.g., Cl<sup>-</sup>, SO<sub>4</sub><sup>2-</sup>, or CO<sub>3</sub><sup>2-</sup>), and *m* is the number of intercalated water molecules.<sup>5</sup> The excellent reducing strength of GRs is attributed to the high Fe<sup>II</sup> content and the fast electron transfer between Fe<sup>II</sup> and Fe<sup>III</sup> in the hydroxide sheets via polaron hopping.<sup>6</sup> The formation of GRs in nature is likely widespread, but due to their rapid oxidation upon exposure to oxygen, identification is difficult.<sup>5</sup>

Green rusts have been synthesized in the laboratory by a variety of approaches such as aerial oxidation of aqueous Fe<sup>II</sup>, coprecipitation, and oxidation of solid Fe(OH)<sub>2</sub>.<sup>7–10</sup> Recently, we have proposed an efficient and robust glycine (Gly)-assisted synthesis method that is fast and scalable, and hence allows for industrial-scale synthesis of GRs. Moreover, modifications to GRs such as the intercalation of organic molecules can make

GRs more reactive toward nonpolar contaminants.<sup>11</sup> Thus, the application of GRs to clean up nonpolar contaminants at the field scale could become feasible.

For in situ soil and groundwater remediation using a reducing agent such as GR, it is important for the particles to disperse efficiently in the contaminated zone (e.g., a plume of chlorinated solvents), without fast passivation (i.e., reactivity loss). This is a problem often observed for zerovalent iron:<sup>12–14</sup> due to its high reducing strength, it also reacts with water<sup>12</sup> and possible other compounds prior to reaching the target site, and thus it will be passivated quickly. GRs, on the other hand, are not as strongly reducing as zerovalent iron (i.e., they are more selective), but they do have a limited E<sub>H</sub>–pH stability, making them susceptible to dissolution and/or transformation to other iron (oxy)hydroxides, such as magnetite.<sup>7</sup> Chloride green rust (GR<sub>Cl</sub>) has been found to be

Received: April 16, 2018

Revised: June 8, 2018

Accepted: June 15, 2018

Published: June 15, 2018

one of the most reactive GRs in terms of pollutant reduction,<sup>2–4</sup> while at the same time also being most susceptible to dissolution and/or transformation processes when exposed to natural waters. Therefore, it would be desirable if the reactivity of GR<sub>Cl</sub> could be controlled or temporarily preserved, to enable homogeneous distribution of GR<sub>Cl</sub> particles across the contaminated site before switching on its reducing potential.

To design an off/on reactivity switch, first a reagent is needed that blocks the GR reactive surface sites to minimize GR dissolution and potential oxidation. Some naturally occurring solutes such as humic acids, silicate, and phosphate have been shown to passivate the reactive surface sites of redox-active iron minerals.<sup>15–20</sup> Of particular interest here is dissolved silica (Si), which is ubiquitous in natural waters and is known to bind strongly to iron oxyhydroxides via surface complexation.<sup>21,22</sup> It has also been demonstrated that the oxidation (i.e., corrosion) of metallic iron can be reduced by Si surface complexation.<sup>23–25</sup> Some studies reported that Si adsorbs to GR surfaces,<sup>26</sup> but to what extent and whether this would stabilize GR and inhibit early reactions with the surrounding aqueous solutes is unknown.

In a second step, to reactivate the GR, the compound used to block the active surface site (e.g., Si) needs to be removed. This can be done either by (i) use of a complexing agent (e.g., F<sup>−</sup> to remove surface sorbed Si), (ii) adding a strong sorbent to desorb Si from the GR surface, (iii) replacement of Si with an electron-conducting sorbate (e.g., an Fe<sup>II</sup> complexant), or (iv) partial GR dissolution to generate new active surface sites. In previous studies, it was shown that Gly complexes with Fe<sup>II</sup> and also enhances GR dissolution;<sup>27,28</sup> thus potentially Gly could remove a blocking agent such as Si. Moreover, Gly was shown to alter the carbon tetrachloride (CT) dehalogenation pathway by suppressing the undesired formation of chloroform (CF).<sup>29</sup> Thus, Gly is hypothesized to reactivate GR stabilized with sorbed Si and simultaneously suppress CF formation.

To design this off/on reactivity switch for GR, the aims of this study were thus two-fold: (1) to investigate whether Si adsorption to GR<sub>Cl</sub> has an effect on GR<sub>Cl</sub> stability and reactivity toward dehalogenation of CT and (2) to assess whether the addition of Gly facilitates reactivation of Si-blocked GR<sub>Cl</sub> toward full CT dehalogenation.

## ■ EXPERIMENTAL SECTION

The general experimental setup is provided in section S1, including chemicals, GR<sub>Cl</sub> synthesis, analytical methods, and data analysis.

**Silica Adsorption.** A 4 mM Si stock solution was prepared by dissolving sodium metasilicate in triple-deionized (TI) water, which was then pH-adjusted to 8.0 by use of HCl. This Si stock solution was diluted with TI water to yield solutions with initial Si concentrations ( $C_0^{\text{Si}}$ ) of 0.05, 0.1, 0.2, 0.4, 0.8, 1.2, 1.6, and 2.0 mM. Aliquots of the washed GR<sub>Cl</sub> (synthesis and washing protocols described in Supporting Information) were resuspended in 10 mL of the prepared Si solutions, to yield final concentrations of 4 mM Fe<sup>II</sup> in GR ( $C_{\text{Fe}^{\text{II}} \text{ GR}}$ ) with  $C_0^{\text{Si}}$  from 0.05 to 2.0 mM. These suspensions were shaken inside an anoxic chamber (Coy Laboratories, Grass Lake, MI) for periods up to 6 days, after which total and aqueous Si concentrations were measured. For one Si concentration (1.6 mM), the time-dependent adsorption of Si to GR was monitored over 140 h in a larger solution volume, where

regular samples were taken for total and aqueous Si measurements.

The Si adsorption data was fitted by use of the Langmuir–Freundlich (Sips) isotherm (eq 1), as well as the two-site Langmuir model (eq 2), to account for other solid phases that may have formed and acted as a secondary sorbent (e.g., magnetite):

$$q = \frac{q_m K C_e^r}{1 + K C_e^r} \quad (1)$$

$$q = \frac{q_{m,1} K_1 C_e}{1 + K_1 C_e} + \frac{q_{m,2} K_2 C_e}{1 + K_2 C_e} \quad (2)$$

In these isotherm equations,  $q$  is the amount of Si adsorbed,  $q_m$  is the maximum adsorption capacity,  $K$  is the equilibrium or affinity constant, and  $C_e$  is the equilibrium concentration of Si in solution after adsorption. In the description of the Langmuir–Freundlich (Sips) isotherm (eq 1), the value of  $r$  is 1 if the adsorption sites are independent and do not interact with each other (corresponds to the Langmuir model). For  $r > 1$ , positive cooperativity is assumed, while for  $0 < r < 1$ , repulsive interactions between sorbates are expected. In the two-site Langmuir isotherm (eq 2), the subscripts 1 and 2 refer to different adsorption sites (sorbents).

**Switch-off GR<sub>Cl</sub> Reactivity: Blockage of Carbon Tetrachloride Dehalogenation.** From the Si adsorption characteristics, a series of experiments was designed to test whether the adsorbed Si limits GR<sub>Cl</sub> reactivity toward CT reduction. Note that a higher GR<sub>Cl</sub> loading ( $C_{\text{Fe}^{\text{II}} \text{ GR}}$  30 mM) was used in these experiments to increase CT reduction rates, and a Si concentration of 4 mM was added to reach maximum Si sorption (i.e., 3 mM Si adsorbed to GR<sub>Cl</sub> and ~1 mM Si in solution). For this, washed GR<sub>Cl</sub> was added to a 4 mM Si solution to yield an initial  $C_{\text{Fe}^{\text{II}} \text{ GR}}$  of 30 mM at pH 8; this solution was then magnetically stirred for 48 h. A number of reactors were set up by transferring 10 mL aliquots of the Si-sorbed GR<sub>Cl</sub> suspension (henceforth called GR<sub>Cl</sub><sup>Si</sup>) into 20 mL glass vials and then adding 50 μL of a 4 mM CT–methanol stock solution to yield 20 μM CT. The vials were immediately sealed with Teflon-lined rubber septa and aluminum crimp caps, taken out of the glovebox, and kept in the dark at room temperature and under constant vertical mixing (15 rpm). Controls of CT without added GR<sub>Cl</sub><sup>Si</sup> and standards of CT and CF in TI water were prepared following the same procedures. Measurements of the GR<sub>Cl</sub><sup>Si</sup> suspension pH prior to addition of CT showed average value of 8.3 ± 0.2, while measurements taken at the end of the reactions, after sampling for organic volatiles, were almost identical, albeit a bit lower at 8.0 ± 0.2. The reaction vials were sacrificed after headspace analysis.

**Reactivation of GR<sub>Cl</sub><sup>Si</sup> for Carbon Tetrachloride Dehalogenation by Use of Glycine.** Different Gly concentrations were added to GR<sub>Cl</sub><sup>Si</sup> to test whether Gly could disable the blocking behavior of the adsorbed Si to enable CT dechlorination. To test this, first a 60 mM GR<sub>Cl</sub><sup>Si</sup> ( $C_{\text{Fe}^{\text{II}} \text{ GR}}$ ) suspension was prepared by concentrating the 30 mM GR<sub>Cl</sub><sup>Si</sup> ( $C_{\text{Fe}^{\text{II}} \text{ GR}}$ ) suspension by centrifugation and removal of half the supernatant volume. Aliquots (5 mL) of 60 mM GR<sub>Cl</sub><sup>Si</sup> ( $C_{\text{Fe}^{\text{II}} \text{ GR}}$ ) suspension were then transferred to a set of 20 mL glass vials and each was amended with Gly stock solution (600 mM, pH 8.0) to yield Gly concentrations of 30, 60, and 120 mM. The vials were then topped up with previously removed supernatant to reach a total volume of 10 mL and a

final  $C_{\text{Fe}^{\text{II}}_{\text{GR}}}$  of 30 mM. Finally, the vials were amended with CT to yield 20  $\mu\text{M}$  and then immediately sealed and incubated as above.

A control experiment was carried out to test CT reduction in the absence of  $\text{GR}_{\text{Cl}}$  in a solution containing 60 mM Gly, 0.5 mM  $\text{Fe}^{\text{II}}$ , 2 mM Si, and 20  $\mu\text{M}$  CT (pH 8.0). The amount of Si and  $\text{Fe}^{\text{II}}$  added to this control experiment was based on concentrations observed in the  $\text{GR}_{\text{Cl}}^{\text{Si}}$  adsorption experiments.

As most groundwaters are carbonate-buffered with near-neutral to alkaline pH, it is possible that  $\text{GR}_{\text{Cl}}$ , once exposed to these waters, may experience chloride interlayer exchange with carbonate, which could decrease GR reactivity.<sup>5</sup> Thus, we tested the effect of carbonate on GR stability and reactivity by amending the Gly reactivation reactors with  $\text{Na}_2\text{CO}_3$  to yield carbonate concentration of 1 and 2 mM. These carbonate concentrations were chosen according to relevant natural bicarbonate/carbonate concentrations in groundwater.

## RESULTS

**Adsorption of Silica on  $\text{GR}_{\text{Cl}}$  and Inhibition of  $\text{Fe}^{\text{II}}$  Dissolution.** The adsorption of Si to  $\text{GR}_{\text{Cl}}$  was tested first to determine the adsorption equilibrium time and maximum adsorption capacity. Figure 1a shows the time-dependent change in Si concentration upon addition of 1.6 mM Si to  $\text{GR}_{\text{Cl}}$  ( $C_{\text{Fe}^{\text{II}}_{\text{GR}}} = 4 \text{ mM}$ ). A very fast removal of Si (i.e., fast Si adsorption) was observed within the first hour, followed by a much slower adsorption process over the following hours and days. The maximum Si sorption measured after 6 days was  $\sim 0.13 (q_{\text{m}}, \text{ mM/mM})$ . X-ray diffraction analysis (XRD) of GR reacted with Si (Figure S2) showed no significant changes in basal plane spacing. This indicated that Si likely adsorbed to external GR particle edge and surface sites, while Si intercalation was less likely, because it would have changed the basal plane spacing.<sup>30</sup>

From the kinetic adsorption experiments, an equilibration time of 6 days was chosen to determine the Si adsorption isotherm at a sorbent concentration of 4 mM  $\text{Fe}^{\text{II}}$  ( $C_{\text{Fe}^{\text{II}}_{\text{GR}}}$ ) with initial Si concentrations ( $C_0^{\text{Si}}$ ) from 0.05 to 2 mM (Figure 1b). At  $C_0^{\text{Si}} \leq 0.4 \text{ mM}$ , all Si adsorbed to GR; that is, no Si could be detected in solution after 6 days. For  $C_0^{\text{Si}} > 0.4 \text{ mM}$ , a clear maximum Si adsorption capacity of  $\sim 0.13 (q_{\text{m}}, \text{ mM/mM})$  (i.e., 0.026 g of Si/g of  $\text{GR}_{\text{Cl}}$ ) was reached, which also indicated a finite number of Si sorption sites on  $\text{GR}_{\text{Cl}}$  particle surfaces (Figure 1b). The Langmuir–Freundlich isotherm (eq 1) was fitted to the data, which provided a maximum adsorption capacity of 0.134 ( $q_{\text{m}}, \text{ mM/mM}$ ), with an equilibrium constant  $K$  of 67.7 L/mmol and  $r$  value of 1.05 ( $R^2 = 0.965$ ). The data were also fitted to the two-site Langmuir model (eq 2) to account for the possible presence of secondary  $\text{Fe}^{\text{II}}$  phases (e.g., magnetite). The fitted maximum adsorption capacities  $q_{\text{m},1}$  and  $q_{\text{m},2}$  were 0.109 and 0.019 (mM/mM), and the equilibrium constants  $K_1$  and  $K_2$  were 752 and 750 L/mmol ( $R^2 = 0.959$ ). Both models suggest a similar adsorption capacity of  $\sim 0.13 (q_{\text{m}}, \text{ mM/mM})$ .

**Blockage of Carbon Tetrachloride Dehalogenation by Silica Adsorption.** The Si adsorption study showed that adsorption equilibrium was reached within 2 days and that the maximum Si adsorption capacity corresponded to a  $C_0^{\text{Si}}/C_{\text{Fe}^{\text{II}}_{\text{GR}}}$  molar ratio of 0.13. This molar ratio was then used in CT dehalogenation experiments to test the impact of adsorbed Si.

In the absence of Si, CT reduction by  $\text{GR}_{\text{Cl}}$  followed pseudo-first-order kinetics ( $k_{\text{obs}} = 2.1 \text{ h}^{-1}$ ) with all added CT

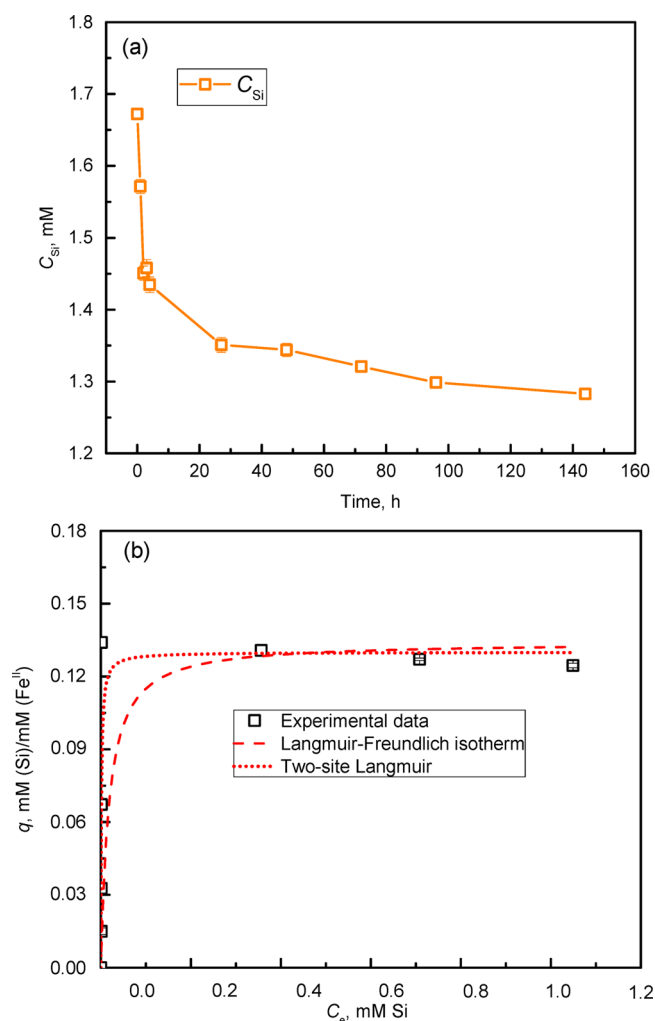


**Figure 1.** (a) Variation in dissolved Si ( $C_{\text{Si}}$ ) during Si adsorption to  $\text{GR}_{\text{Cl}}$  ( $C_{\text{Fe}^{\text{II}}_{\text{GR}}} = 4 \text{ mM}$  and  $C_0^{\text{Si}} = 1.6 \text{ mM}$ , pH 8.0). (b) Adsorption isotherm of Si adsorption on  $\text{GR}_{\text{Cl}}$  for 6 days of equilibration time ( $C_{\text{Fe}^{\text{II}}_{\text{GR}}} = 4 \text{ mM}$ , pH 8.0). Error bars represent the standard deviation ( $n = 3$ ). Dashed lines show fits to the Langmuir–Freundlich (Sips) isotherm and two-site Langmuir model.

being reduced within 3 h (Figure 2). The dominant product that formed was CF (77%), with the remainder being CO and HCOOH (Table 1). In contrast, at a  $C_0^{\text{Si}}/C_{\text{Fe}^{\text{II}}_{\text{GR}}}$  molar ratio of 0.13, CT dehalogenation seemed strongly inhibited, with only a small amount of CT ( $\sim 16\%$ ) removed after 48 h of monitoring. Interestingly, however, no dehalogenation products (i.e., CF, CO, and formic acid) could be detected. This may indicate that the loss of CT occurred due to CT adsorption to the nonreactive  $\text{GR}_{\text{Cl}}^{\text{Si}}$ .

In terms of dissolution behavior during the dehalogenation experiment; in the absence of Si, GR released approximately 2.2 mM  $\text{Fe}^{\text{II}}$  during the first day, but not much more thereafter (Figure S3). Under conditions of maximum Si adsorption to  $\text{GR}_{\text{Cl}}$  ( $\sim 0.13 C_0^{\text{Si}}/C_{\text{Fe}^{\text{II}}_{\text{GR}}}$  molar ratio),  $\text{GR}_{\text{Cl}}$  dissolution was several orders of magnitude lower, with only 0.09 mM  $\text{Fe}^{\text{II}}$  released after 2 days (Figure S3). These results clearly show that the overall dissolution rate was dramatically reduced by the sorption of Si.

**Reactivation of Carbon Tetrachloride Dehalogenation.** Glycine was added to  $\text{GR}_{\text{Cl}}^{\text{Si}}$  to test whether it can reactivate CT dehalogenation. Figure 3 shows that CT

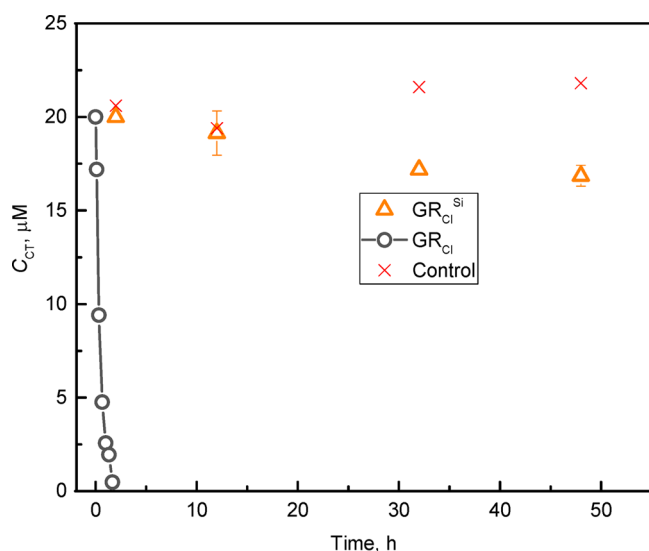


**Figure 2.** Comparison of CT dehalogenation by GR<sub>Cl</sub> and GR<sub>Cl</sub><sup>Si</sup> ( $C_{\text{Fe}^{\text{II}}_{\text{GR}}} = 30 \text{ mM}$ ,  $C_0^{\text{Si}} = 4 \text{ mM}$ , and  $C_0^{\text{CT}} = 20 \text{ } \mu\text{M}$ ). Control experiments contained no GR<sub>Cl</sub> but all other components: 0.5 mM Fe<sup>II</sup>, 20  $\mu\text{M}$  CT, 2 mM Si, and 60 mM Gly. Solid line shows pseudo-first-order rate fitting. Error bars represent the standard deviation ( $n = 3$ ).

dehalogenation can indeed be reactivated by the addition of Gly, with over 95% of the CT removed within 48 h under all tested Gly conditions. The reduction rate slightly increased with increasing Gly concentrations, with  $k_{\text{obs}}$  increasing from  $0.75 \times 10^{-1}$  (at 30 mM Gly) to  $1.1 \times 10^{-1} \text{ h}^{-1}$  (at 120 mM Gly; Table 1). The main products were CF, CO, and HCOOH at all tested Gly concentrations, but the CF proportion notably decreased with increasing Gly (Table 1).

**Interaction between GR<sub>Cl</sub><sup>Si</sup> and Glycine.** To assess whether Gly addition enhanced GR<sub>Cl</sub><sup>Si</sup> dissolution, 60 mM Gly was added to GR<sub>Cl</sub><sup>Si</sup> (in the absence of CT) and the amounts of dissolved Si ( $C_{\text{Si}}$ ) and Fe ( $C_{\text{Fe}}$ ) were regularly measured over 48 h. Over this time,  $C_{\text{Si}}$  showed a decline from 0.89 to 0.69 mM, while  $C_{\text{Fe}}$  increased from 0.07 to 0.21 mM (Figure 4). In the absence of Gly,  $C_{\text{Si}}$  and  $C_{\text{Fe}}$  remained relatively stable around 0.98 mM and 0.08 mM, respectively (Figure 4). This trend was also confirmed in a separate set of experiments, where GR<sub>Cl</sub><sup>Si</sup> was exposed to all tested Gly concentrations but for a total length of 6 days: with an increase in Gly concentration from 0 to 120 mM Gly,  $C_{\text{Fe}}$  increased from 0.09 to 8.1 mM and  $C_{\text{Si}}$  decreased from 0.74 to 0.06 mM (Figure S4a). Thus, the addition of Gly led to a significant

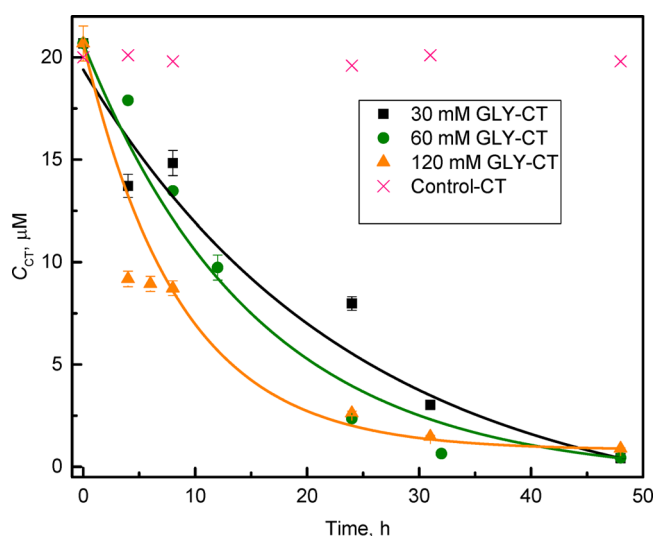


**Figure 3.** Reactivation of GR<sub>Cl</sub><sup>Si</sup> for CT dehalogenation by addition of 30, 60, and 120 mM Gly ( $C_{\text{Fe}^{\text{II}}_{\text{GR}}} = 30 \text{ mM}$ ,  $C_0^{\text{Si}} = 4 \text{ mM}$ ,  $C_0^{\text{CT}} = 20 \text{ } \mu\text{M}$ , pH 8). The control is Fe<sup>II</sup>-Si-Gly-CT matrix (cf. Figure 2). Error bars represent the standard deviation ( $n = 3$ ).

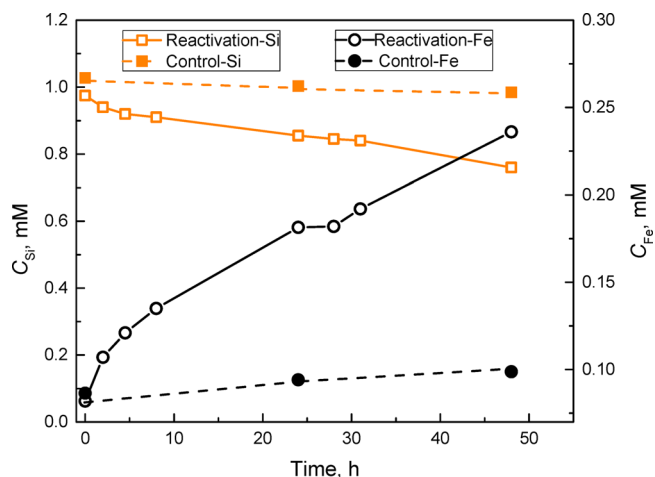


**Figure 4.** Si and Fe concentrations in solution after reactivation by Gly ( $C_{\text{Fe}^{\text{II}}_{\text{GR}}} = 30 \text{ mM}$ ,  $C_0^{\text{Si}} = 4 \text{ mM}$ , 60 mM Gly, pH 8). The control reaction contains GR<sub>Cl</sub><sup>Si</sup> only, without Gly. The pH in all experiments was around 8.0.

increase in GR<sub>Cl</sub><sup>Si</sup> dissolution, while the decrease in dissolved Si was probably due to sorption and/or precipitation. To test only for the interaction between dissolved Si, Fe, and Gly, a set

**Table 1. Kinetics and Dehalogenation Products for Green Rust Reduction of Carbon Tetrachloride<sup>a</sup>**

GR type	Gly (mM)	$k_{\text{obs}}$ (h <sup>-1</sup> )	$t_{\text{R}}^b$ (h)	product distribution (%)			
				CF	CO	HCOOH	total <sup>c</sup>
GR <sub>Cl</sub> <sup>d</sup>	0	2.10 ± 0.1	24	77.0	1.46	19.5	98.6 ± 2.6
GR <sub>Cl</sub> <sup>e</sup>	60	0.7 ± 0.0	24	8.9	29.5	71.5	109.0 ± 9.5
GR <sub>Cl</sub> <sup>Si</sup>	0	<i>f</i>	72	0	<i>g</i>	<i>g</i>	<i>f</i>
GR <sub>Cl</sub> <sup>Si</sup>	30	0.075 ± 0.01	72	60.0	30.1	10.1	100.0 ± 5.1
GR <sub>Cl</sub> <sup>Si</sup>	60	0.096 ± 0.004	72	51.5	32.0	14.2	97.7 ± 3.5
GR <sub>Cl</sub> <sup>Si</sup>	120	0.11 ± 0.01	72	27.0	33.9	36.6	97.5 ± 4.6

<sup>a</sup>Measured in the absence of Si, after Si blocking, and after reactivation with glycine.  $C_{\text{Fe}^{\text{II}}_{\text{GR}}} = 30 \text{ mM}$ ;  $C_0^{\text{CT}} = 20 \text{ } \mu\text{M}$ . <sup>b</sup>Reaction time where CT was completely removed. <sup>c</sup>Error:  $e_{\text{total}} = [(e_{\text{CF}}^2 + e_{\text{CO}}^2 + e_{\text{HCOOH}}^2)/3]^{1/2}$ . <sup>d</sup>Control reaction with GR<sub>Cl</sub> without Si adsorption. <sup>e</sup>Control reaction with GR<sub>Cl</sub> with 60 mM Gly. <sup>f</sup>No reaction. <sup>g</sup>Not detected.

of control experiments were carried out, where Gly and  $C_{Si}$  were fixed at 60 and 0.5 mM, respectively, and  $C_{Fe}$  was varied (Figure S4b). These showed that the more aqueous  $Fe^{II}$  was added, the more Si and  $Fe^{II}$  were removed from solution after 6 days, indicating possible formation of Si- $Fe^{II}$  precipitates.

Seeing that Gly increased the solubility of  $GR_{Cl}^{Si}$  (Figure 4), we also examined the Gly-reactivated  $GR_{Cl}^{Si}$  with XRD and transmission electron microscopy (TEM) after 6 days of reaction time. The XRD patterns showed a marked decrease in  $GR_{Cl}^{Si}$  crystallinity with increasing Gly from 0 to 120 mM, demonstrated by the broadening of the basal plane reflections. At 120 mM Gly, reflections for magnetite appeared, demonstrating partial transformation of  $GR_{Cl}$  to magnetite (Figure 5). Even though CT reduction by  $GR_{Cl}^{Si}$  still

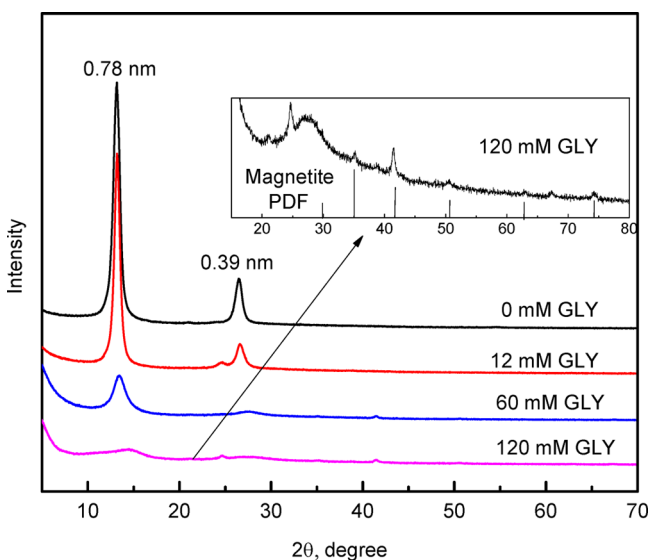


**Figure 5.** XRD patterns of  $GR_{Cl}^{Si}$  exposed to different Gly concentrations for 6 days ( $C_{Fe}^{II}{}_{GR} = 30$  mM,  $C_0^{Si} = 4$  mM, pH 8). (Inset) Magnetite formation in the presence of Gly.

completed in the presence of 120 mM Gly (Figure 3), the high Gly content induced intensive  $GR_{Cl}$  dissolution, and hence the switch function might be lost. TEM observations confirmed the trends seen in XRD. The pure  $GR_{Cl}^{Si}$  sample (no added Gly) showed the typical platy and hexagonal morphology of GR particles (Figure 6a), with some smaller particles that could likely be Si precipitates. In the presence of 60 mM Gly, GR particles were more fragmented, with smaller

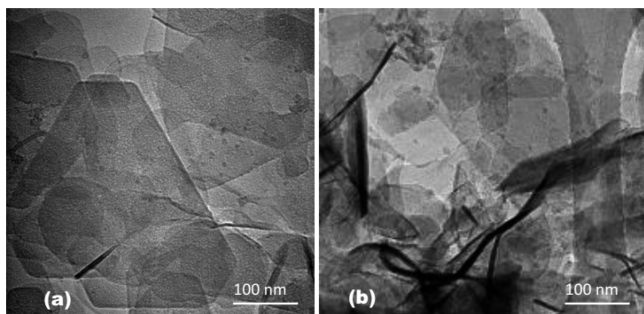


**Figure 6.** TEM images of (a)  $GR_{Cl}^{Si}$  exposed to TI water for 6 days and (b)  $GR_{Cl}^{Si}$  exposed to 60 mM Gly for 6 days (all at pH  $\approx$  8).

sizes and more rounded shapes (Figures 6b), as expected from the enhanced dissolution in the presence of Gly.

**Effects of Carbonate on Reactivation of  $GR_{Cl}^{Si}$ .** Pore waters in contaminated sediments and aquifers often have substantial alkalinity. Carbonate and bicarbonate are strongly sorbed by GRs, which causes exchange of interlayer  $Cl^-$  and formation of the carbonate form of GR ( $GR_{CO_3}$ ). The  $GR_{CO_3}$  may be less reactive than  $GR_{Cl}$ , and thus we tested the reactivation of  $GR_{Cl}^{Si}$  in the presence of 1 and 2 mM carbonate (Figure 7). It is seen that the presence of bicarbonate retards CT dehalogenation and almost impedes the reactivation at a concentration of 2 mM bicarbonate.

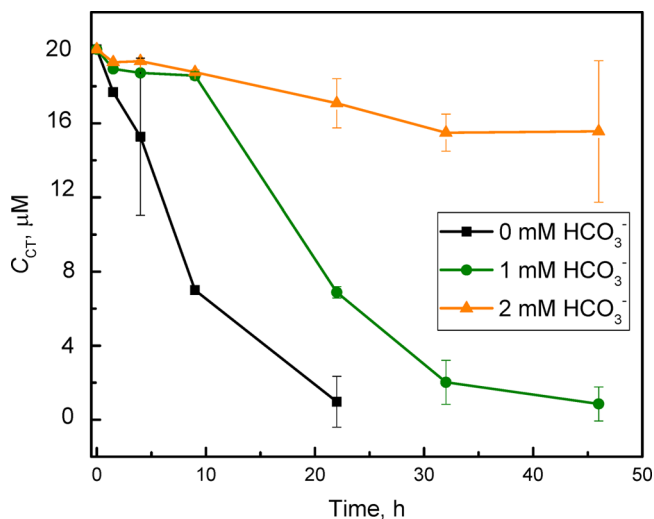


**Figure 7.** Reactivation of CT dehalogenation of  $GR_{Cl}^{Si}$  in the presence of 30 mM Gly and two different bicarbonate concentrations ( $C_{Fe}^{II}{}_{GR} = 30$  mM,  $C_0^{Si} = 4$  mM, pH 8). Error bars represent the standard deviation ( $n = 3$ ).

## DISCUSSION

**Interaction between Silicate and  $Fe^{II}$ .** A decrease in dissolved Si ( $C_{Si}$ ) was observed with increasing GR dissolution induced by the addition of Gly (Figure 4). This indicated that more Si adsorbed or precipitated, for example, to strongly sorbing secondary iron phases (e.g., magnetite or ferrihydrite) that may have formed during GR dissolution and/or that Si precipitated along with  $Fe^{II}$ , for example, as iron(II) silicates. The latter process was also suggested by the set of control experiments performed with fixed Gly (60 mM) and  $C_{Si}$  (0.5 mM), and varied initial  $Fe^{II}$  concentrations ( $C_{Fe} = 0$ –0.5 mM), which showed that both  $C_{Si}$  and  $C_{Fe}$  decreased (i.e., precipitated) with increasing initial  $Fe^{II}$  (Figure S4b). This indicated the possible formation of  $Fe^{II}$ -Si precipitates with a Fe/Si molar ratio of  $2.03 \pm 0.29$ .<sup>31–33</sup> Moreover, Minteq calculations showed that these control experiments were oversaturated with respect to the clay silicate greenalite [ $Fe^{II}/Si$  (mM/mM)  $\approx$  1.5] (Table S1); hence the formation of greenalite was thermodynamically possible. Tosca et al.<sup>34</sup> demonstrated the formation of hydrous iron<sup>II</sup>-silicate gel in artificial seawater after 10 days of reaction time (at 25 °C, pH 8.0), which with time, will likely crystallize to greenalite.

**$GR_{Cl}$  Reactivity Switch-off by Silica Adsorption.** At low Si loading ( $C_0^{Si}/C_{Fe}^{II}{}_{GR} < 1.3$ ),  $GR_{Cl}$  partly transformed to other solids such as magnetite because of high solubility of

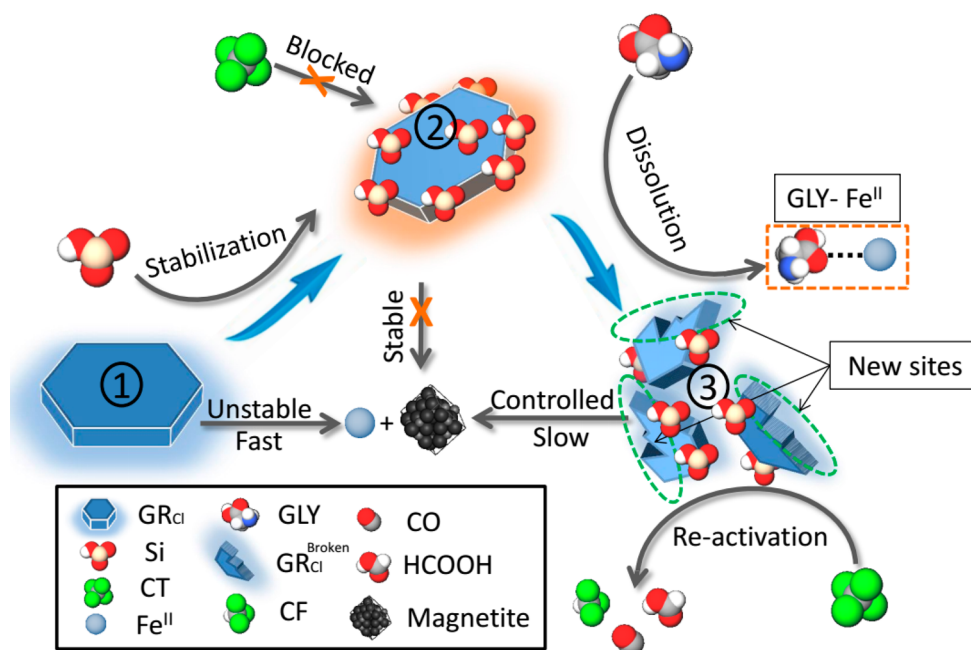


**Figure 8.** Schematic diagram of the switch mechanism. Phase ① is original  $\text{GR}_{\text{Cl}}$ , which is not stable because of dissolution and transformation to magnetite. In phase ②, Si adsorption on  $\text{GR}_{\text{Cl}}$  blocks CT reduction and inhibits  $\text{GR}_{\text{Cl}}$  dissolution. In phase ③, CT dehalogenation is reactivated by Gly due to breakdown of  $\text{GR}_{\text{Cl}}$  and generation of new reactive sites.

$\text{GR}_{\text{Cl}}$ , which is also well-known from other studies<sup>29</sup> (Figure S3). Magnetite formation is also indicated by color changes of the suspensions, turning from dark green/blue to black, during the adsorption experiment. It is expected that Si also sorbed to magnetite. At higher Si loading ( $C_0^{\text{Si}}/C_{\text{Fe}^{\text{II}}_{\text{GR}}} > 1.3$ ), Si adsorption stabilized  $\text{GR}_{\text{Cl}}$ , also confirmed by the absence of magnetite formation because the suspension color remained dark green/blue and there were no magnetite peaks in XRD patterns (Figure S2). Even though  $\text{Fe}^{\text{II}}\text{-Si}$  precipitates may have formed, the amount of that  $\text{Fe-Si}$  phase (gel, amorphous, or crystalline) would have been much lower than the added GR mass (Figure 1), and thus its impact would have been low.

On the basis of approximate particle sizes of  $\text{GR}_{\text{Cl}}$  as determined by TEM (Figure 6) and XRD (Figure 5), we estimated the density of OH groups on  $\text{GR}_{\text{Cl}}$  particle surfaces (section S2). The calculations showed that the maximum Si adsorption density observed here (Figure 1b) was approximately equal to the density of total OH sites on the  $\text{GR}_{\text{Cl}}$  particle surface, suggesting both outer edge and planar sites were blocked by adsorbed Si. In addition, as the  $r$  value in the Sips isotherm model is close to 1, this adsorption may be interpreted as a monolayer adsorption process. Therefore, CT reduction was effectively suppressed because CT could not access the reactive OH sites where Si adsorbed. It has been reported that contaminants might be reduced only at GR edge sites and not at planar sites.<sup>6,35,36</sup> However, with the data at hand, it is not possible to deduce if CT reduction occurred only at edge sites. It is worth noting that the amount of dissolved GR (i.e.,  $\text{Fe}^{\text{II}}$ ) at maximum Si loading was only 0.09 mM after 48 h (Figure S3), while in the absence of Si, substantially more GR dissolved (dissolved  $\text{Fe}^{\text{II}}$  around 2.5 mM). Thus, GR site blocking by Si not only inhibits CT adsorption and hence degradation but also stabilizes  $\text{GR}_{\text{Cl}}$  against dissolution and transformation. This is an important finding, particularly in terms of its potential use for soil and groundwater remediation through injection.

**$\text{GR}_{\text{Cl}}$  Reactivity Switch-on by Glycine.** The changes in dissolved Si and Fe after addition of Gly suggest the occurrence of the following interactions between Gly and  $\text{GR}_{\text{Cl}}^{\text{Si}}$ , which eventually led to the reactivation of GR (Figure 8): Gly dissolves  $\text{GR}_{\text{Cl}}^{\text{Si}}$  (producing aqueous  $\text{Fe}^{\text{II}}$ ), which triggers GR fragmentation into smaller particles and transformation to magnetite (particularly at high Gly concentrations); this ultimately generates new reactive sites for CT dehalogenation. According to our previous study, the presence of Gly reduces the formation of CF during CT dehalogenation by  $\text{GR}_{\text{Cl}}^{\text{Si}}$ .<sup>29</sup> However, here a fairly large proportion of CF still formed during reactivation of  $\text{GR}_{\text{Cl}}^{\text{Si}}$  with Gly, indicating that Si might also affect the dehalogenation pathway.

**Environmental Implications.** Remediation of polluted soils and groundwater requires reactivity control during injection and distribution of the reducing reagent in the targeted contaminated subsurface. In the case of using GR for this application, care also must be taken to avoid GR dissolution and unnecessary oxidation (e.g., during mixing with sediments). This study demonstrates that it is possible to control the stability and reactivity of  $\text{GR}_{\text{Cl}}$ . The dissolution of  $\text{GR}_{\text{Cl}}$  and the dehalogenation of CT can be almost completely inhibited through Si adsorption. Once successfully distributed in the subsurface, CT dehalogenation can then be turned on again by exposure to Gly. This stepwise application of Si and then Gly may work equally well as a reactivity off/on switch for other reactive Fe solids used for chlorinated solvent cleanup (e.g., zerovalent iron). However, more work is required to optimize this reactivity switch, particularly testing of interactions between GR and other solids and solutes that could be present when GR is injected into contaminated soils and groundwater. As an example, we showed here that water alkalinity can have a marked effect on this reactivity switch, particularly at alkalinities  $>1$  mM. Overall, our study demonstrates that it is possible to develop efficient and realistic switches by use of nontoxic agents, which represents

an important step in overcoming challenges with dispersion and reactivity loss during application of iron-based materials for groundwater remediation.

## ■ ASSOCIATED CONTENT

### Supporting Information

The Supporting Information is available free of charge on the ACS Publications website at DOI: 10.1021/acs.est.8b02020.

Additional text sections describing general experimental setup and calculation of Fe-OH site density; four figures showing molecular model of GR, XRD patterns, release of Fe<sup>II</sup> as a result of GR<sub>Cl</sub> dissolution, and Fe and Si solution concentrations; one table listing Minteq calculations of interactions (PDF)

## ■ AUTHOR INFORMATION

### Corresponding Author

\*E-mail lizhihuang@whu.edu.cn.

### ORCID

Weizhao Yin: 0000-0003-4411-1821

Li-Zhi Huang: 0000-0001-8222-5139

Dominique J. Tobler: 0000-0001-8532-1855

Hans Christian B. Hansen: 0000-0002-8617-2393

### Notes

The authors declare no competing financial interest.

## ■ ACKNOWLEDGMENTS

We thank the Fundamental Research Funds for the Central Universities (21618343), Guangzhou Elite Plan (JY201305), Danish Research Council (Grant 274-09-0360) within the research project "Iron hydroxide intercalates for degradation of halogenated solvents in sediments and groundwater" (Iron-X), Danish Council for Independent Research, DFF-Individual postdoctoral grants (DFF-4093-00295), and Start-up Fund for Distinguished Scholars, Wuhan University (1403-413100041) for their support.

## ■ REFERENCES

- (1) Ayala-Luis, K. B.; Cooper, N. G.; Koch, C. B.; Hansen, H. C. Efficient dechlorination of carbon tetrachloride by hydrophobic green rust intercalated with dodecanoate anions. *Environ. Sci. Technol.* **2012**, *46* (6), 3390–7.
- (2) Choi, J.; Batchelor, B.; Chung, J. Reductive dechlorination of tetrachloroethylene by green rusts modified with copper. *Water, Air, Soil Pollut.* **2010**, *212* (1–4), 407–417.
- (3) Liang, X.; Butler, E. C. Effects of natural organic matter model compounds on the transformation of carbon tetrachloride by chloride green rust. *Water Res.* **2010**, *44* (7), 2125–32.
- (4) Liang, X.; Philp, R. P.; Butler, E. C. Kinetic and isotope analyses of tetrachloroethylene and trichloroethylene degradation by model Fe(II)-bearing minerals. *Chemosphere* **2009**, *75* (1), 63–69.
- (5) Génin, J.-M. R.; Bourrié, G.; Trolard, F.; Abdelmoula, M.; Jaffrezic, A.; Refait, P.; Maitre, V.; Humbert, B.; Herbillon, A. Thermodynamic equilibria in aqueous suspensions of synthetic and natural Fe (II)-Fe (III) green rusts: occurrences of the mineral in hydromorphic soils. *Environ. Sci. Technol.* **1998**, *32* (8), 1058–1068.
- (6) Wander, M. C.; Rosso, K. M.; Schoonen, M. A. Structure and charge hopping dynamics in green rust. *J. Phys. Chem. C* **2007**, *111* (30), 11414–11423.
- (7) Ruby, C.; Aissa, R.; Géhin, A.; Cortot, J.; Abdelmoula, M.; Génin, J.-M. Green rusts synthesis by coprecipitation of Fe<sup>II</sup>-Fe<sup>III</sup> ions and mass-balance diagram. *C. R. Geosci.* **2006**, *338* (6–7), 420–432.

(8) Antony, H.; Labrit, A.; Rouchaud, J. C.; Legrand, L.; Chaussé, A. Study of Fe<sup>II</sup>/Fe<sup>III</sup> ratio in thin films of carbonate or sulphate green rusts obtained by potentiostatic electrosynthesis. *Electrochim. Acta* **2008**, *53* (24), 7173–7181.

(9) Drissi, H.; Refait, P.; Génin, J.-M. The oxidation of Fe (OH)<sub>2</sub> in the presence of carbonate ions: structure of carbonate green rust one. *Hyperfine Interact.* **1994**, *90* (1), 395–400.

(10) Usman, M.; Hanna, K.; Abdelmoula, M.; Zegeye, A.; Faure, P.; Ruby, C. Formation of green rust via mineralogical transformation of ferric oxides (ferrihydrite, goethite and hematite). *Appl. Clay Sci.* **2012**, *64*, 38–43.

(11) Huang, L. Single Sheet Metal Oxides and Hydroxides: Synthesis, Properties and Applications. Ph.D. Thesis, Department of Plant and Environmental Sciences, Faculty of Science, University of Copenhagen, 2013; [https://research.ku.dk/search/?pure=en/publications/single-sheet-metal-oxides-and-hydroxides\(acdcf40a-82a7-4caf-8f43-cea96a4f2562\).html](https://research.ku.dk/search/?pure=en/publications/single-sheet-metal-oxides-and-hydroxides(acdcf40a-82a7-4caf-8f43-cea96a4f2562).html).

(12) Tratnyek, P. G.; Johnson, R. L.; Lowry, G. V.; Brown, R. A. In situ chemical reduction for source remediation. In *chlorinated solvent source zone remediation*; Springer: New York, 2014; pp 307–351; DOI: 10.1007/978-1-4614-6922-3\_10.

(13) Suthersan, S. S. *Remediation engineering: Design concepts*; CRC Press, 1996.

(14) Stroo, H. F.; Ward, C. H. *In situ remediation of chlorinated solvent plumes*; Springer Science & Business Media, 2010; DOI: 10.1007/978-1-4419-1401-9.

(15) Yin, W.; Wu, J.; Li, P.; Wang, X.; Zhu, N.; Wu, P.; Yang, B. Experimental study of zero-valent iron induced nitrobenzene reduction in groundwater: The effects of pH, iron dosage, oxygen and common dissolved anions. *Chem. Eng. J.* **2012**, *184*, 198–204.

(16) Klausen, J.; Vikesland, P. J.; Kohn, T.; Burris, D. R.; Ball, W. P.; Roberts, A. L. Longevity of granular iron in groundwater treatment processes: solution composition effects on reduction of organohalides and nitroaromatic compounds. *Environ. Sci. Technol.* **2003**, *37* (6), 1208–1218.

(17) Le, C.; Wu, J.; Deng, S.; Li, P.; Wang, X.; Zhu, N.; Wu, P. Effects of common dissolved anions on the reduction of para-chloronitrobenzene by zero-valent iron in groundwater. *Water Sci. Technol.* **2011**, *63* (7), 1485–1490.

(18) Su, C.; Puls, R. W. Arsenate and arsenite removal by zerovalent iron: effects of phosphate, silicate, carbonate, borate, sulfate, chromate, molybdate, and nitrate, relative to chloride. *Environ. Sci. Technol.* **2001**, *35* (22), 4562–4568.

(19) Armstrong, R.; Zhou, S. The corrosion inhibition of iron by silicate related materials. *Corros. Sci.* **1988**, *28* (12), 1177–1181.

(20) Remy, P.-P.; Etique, M.; Hazotte, A.; Sergent, A.-S.; Estrade, N.; Cloquet, C.; Hanna, K.; Jorand, F. Pseudo-first-order reaction of chemically and biologically formed green rusts with Hg<sup>II</sup> and C<sub>15</sub>H<sub>15</sub>N<sub>3</sub>O<sub>2</sub>: Effects of pH and stabilizing agents (phosphate, silicate, polyacrylic acid, and bacterial cells). *Water Res.* **2015**, *70*, 266–278.

(21) Gunnarsson, I.; Arnórsson, S. Amorphous silica solubility and the thermodynamic properties of H<sub>4</sub>SiO<sub>4</sub> in the range of 0 to 350°C at P sat. *Geochim. Cosmochim. Acta* **2000**, *64* (13), 2295–2307.

(22) Beckwith, R.; Reeve, R. Studies on soluble silica in soils. I. The sorption of silicic acid by soils and minerals. *Aust. J. Soil Res.* **1963**, *1* (2), 157–168.

(23) Roberts, L. C.; Hug, S. J.; Ruettimann, T.; Billah, M. M.; Khan, A. W.; Rahman, M. T. Arsenic removal with iron (II) and iron (III) in waters with high silicate and phosphate concentrations. *Environ. Sci. Technol.* **2004**, *38* (1), 307–315.

(24) Keith, P. D. A.; Lai, C.; Kjeldsen, P.; Lo, I. M. Effect of groundwater inorganics on the reductive dechlorination of TCE by zero-valent iron. *Water, Air, Soil Pollut.* **2005**, *162* (1–4), 401–420.

(25) Rushing, J. C.; McNeill, L. S.; Edwards, M. Some effects of aqueous silica on the corrosion of iron. *Water Res.* **2003**, *37* (5), 1080–1090.

(26) Ruby, C.; Gehin, A.; Aissa, R.; Ghanbaja, J.; Abdelmoula, M.; Génin, J.-M. R. Chemical stability of hydroxysulphate green rust

synthesised in the presence of foreign anions: carbonate, phosphate and silicate. *ICAME 2005* **2006**, 803–807.

(27) Yin, W.; Huang, L.; Pedersen, E. B.; Frandsen, C.; Hansen, H. C. B. Glycine buffered synthesis of layered iron(II)-iron(III) hydroxides (green rusts). *J. Colloid Interface Sci.* **2017**, *497*, 429–438.

(28) Hertrampf; Olivares. Iron amino acid chelates. *Int. J. Vitam. Nutr. Res.* **2004**, *74* (6), 435–443.

(29) Yin, W.; Strobel, B.; Hansen, H. C. B. Amino acid assisted dehalogenation of carbon tetrachloride by green rust: inhibition of chloroform production. *Environ. Sci. Technol.* **2017**, *51*, 3445–3452.

(30) Del Arco, M.; Gutierrez, S.; Martin, C.; Rives, V.; Rocha, J. Effect of the Mg: Al ratio on borate (or silicate)/nitrate exchange in hydrocalcite. *J. Solid State Chem.* **2000**, *151* (2), 272–280.

(31) Konhauser, K.; Ferris, F. Diversity of iron and silica precipitation by microbial mats in hydrothermal waters, Iceland: Implications for Precambrian iron formations. *Geology* **1996**, *24* (4), 323–326.

(32) Sjöberg, S. Silica in aqueous environments. *J. Non-Cryst. Solids* **1996**, *196*, 51–57.

(33) Kudielka, H. Crystal-structure of Fe<sub>2</sub>Si, its relationship to ordered structures of alpha-(Fe, Si) mixed-crystal and to Fe<sub>3</sub>Se<sub>3</sub> structure. *Z. Kristallogr. - Cryst. Mater.* **1977**, *145* (3–4), 177–189.

(34) Tosca, N. J.; Guggenheim, S.; Pufahl, P. K. An authigenic origin for Precambrian greenalite: Implications for iron formation and the chemistry of ancient seawater. *Geol. Soc. Am. Bull.* **2016**, *128* (3–4), 511–530.

(35) Hansen, H. C. B.; Koch, C. B.; Nancke-Krogh, H.; Borggaard, O. K.; Sørensen, J. Abiotic nitrate reduction to ammonium: key role of green rust. *Environ. Sci. Technol.* **1996**, *30* (6), 2053–2056.

(36) Hansen, H. C. B.; Guldberg, S.; Erbs, M.; Koch, C. B. Kinetics of nitrate reduction by green rusts—effects of interlayer anion and Fe (II): Fe (III) ratio. *Appl. Clay Sci.* **2001**, *18* (1-2), 81–91.